33RD CONGRESS
OF THE INTERNATIONAL COUNCIL
OF THE AERONAUTICAL SCIENCES
STOCKHOLM, SWEDEN, 4–9 SEPTEMBER, 2022

ICAS 2022 SWEDEN

AERODYNAMIC CHARACTERISTICS OF BOX WINGS FOR AN INNOVATIVE EVTOL CONFIGURATION

SHIMA Eiji[1], YONEZAWA Koichi[2], NISHIDA Ryoma[3], HONDA Shusuke & SATO Makoto[3]

[1]Japan Aerospace Exploration Agency, Japan
[2]Central Research Institute of Electric Power Industry, Japan
[3]Kogakuin University, Japan

Abstract

In recent years, electric vertical take-off and landing aircraft (eVTOL), such as electric multicopter, have expanded their applications, and a considerable number of aircraft for human transportation are currently being planned. Among them, the convertible eVTOL (CeVTOL), which cruises using a fixed-wing and has a higher lift-drag ratio, has been attracting attention. The purpose of this study is to understand the aerodynamic characteristics of box wings by wind tunnel experiments to realize an innovative eVTOL that is lightweight and simple by maximizing the features of electric multicopter. From the experimental results, it was found that box wings have characteristics suitable for a convertible VTOL, such as low drag near cruise due to low induced drag compared to a normal cantilever wing with the same wing area and wingspan, and low drag during transition flight due to its small frontal projected area.

Keywords: Wind tunnel test, CFD, powered-lift, Multicopter, Convertible VTOL

1. Introduction

In recent years, electric vertical take-off and landing aircraft (eVTOL), such as electric multicopter, have expanded their applications, and a considerable number of aircraft for human transportation are currently being planned. Among them, the convertible eVTOL (CeVTOL), which cruises using a fixed-wing and has a high lift-drag ratio, has been attracting attention due to its higher cruise performance.

Shima et al. [1,2] proposed the Passive Pendulum Body concept (PPB) as a new type of convertible eVTOL, which is similar to the tilt-wing configuration, but the angle between the wing and the fuselage is not actively moved by the actuator. The fuselage is suspended via a freely rotating single axis, and the fuselage is maintained in a horizontal attitude passively by gravity when hovering, and by a horizontal stabilizer in addition for forward flight. The PPB configuration is as simple as a pure multicopter since all thrust and control moments are given by propellers. This configuration is made possible by utilizing the high agility of the multicopter. See Figure1.

It has been demonstrated that a radio-controlled model (see Figure 2) that uses the same control unit of a multicopter and no other control surfaces can perform stable conversion flight and horizontal flight.

The common aerodynamic problem of both PPB and tilt wings is the gap between the wing and the fuselage that is necessary for wing rotation, and the air leakage from the gap reduces the efficiency of the wing. In order to solve this problem, we have produced a novel PPB with a box wing (PPBB) configuration, which uses a box-shaped wing that surrounds the propellers of a multicopter.

By using the box wing, the left and right wings become continuous and there is no gap between them. In addition, the box wing is known to have a higher wing efficiency than a normal cantilever wing.[3] It also has the potential to achieve higher strength and rigidity with a lightweight structure.

The purpose of this study is to understand the aerodynamic characteristics of the PPBB configuration in the hovering, transition, and cruise conditions by wind tunnel experiments. The wind tunnel models with propellers and the ability to change the wing angle while keeping the fuselage horizontal (Figure 3) were used to measure the longitudinal forces and a moment by varying the attitude angle, propeller

speed, and wind tunnel velocity. Four types of box wings with different wing cross-sectional shapes and a cantilever wing for comparison were used as the wing shapes.

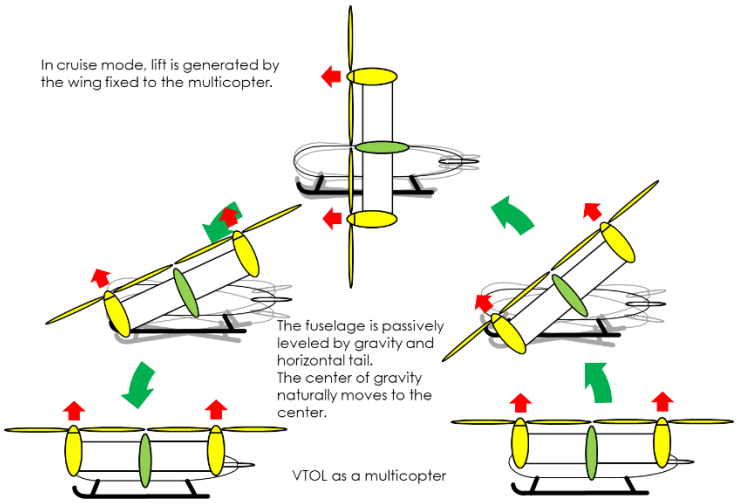

Figure 1 - Illustration on transition flight of the PPB configuration

Figure 2 - Radio Controlled Flight Model for PPB Configuration

Figure 3 – Motion of the box wing test model

2. Wind Tunnel Test

2.1 Wind Tunnel

We used the Planetary Environment Wind Tunnel owned by the Institute of Space and Astronautical Science of the Japan Aerospace Exploration Agency. This facility is a closed-circuit wind tunnel that can be operated in a depressurized environment, but this time the tests were conducted under atmospheric pressure. The outlet of the measurement section is an open-jet type, circular in shape with a diameter of 1.6 m, and there is a suction outlet with a diameter of 1.9 m, 3.5 m backward downstream from the outlet. The wind speeds were set to 10 m/s and 20 m/s.

2.2 Wind Tunnel Test Models

Frontal views of the models are illustrated in Figure 4, the dimensions are shown in Table 1 and the computer graphics of the models are shown in Figure 5.

The box wings and the cantilever wing share common motors, propellers, frames, and a body. A rotary actuator and a six components balance is stored in the body and the balance measure forces and moments acting on only wings, frames, and propellers excluding forces acting on the body.

Wing2421 is the cantilever wing using NACA2421 airfoil which have 21% thickness, Box2421 is the box wing using NACA2421 airfoil and Box0012 is the box wing using NACA0012 airfoil which have 12% thickness. The gurney flaps that height is 5mm are set on the trailing edge of the upper and lower wings of Box2421_flap and Box0012_flap configurations.

The airfoils of Wing2421, Box0012 and Box0012_flap are set parallel to their motor axis, on the other hand, the airfoil of Box2421 and Box2421_flap has a 20-degree downward angle of attack, so lift is generated downward at a 0-degree angle of attack.

Each wing was manufactured by additive manufacturing using resin, and the surface is not smooth. It may increase aerodynamic drag and decrease lift, however, the quantitative amount is not known at this point.

Four motors and propellers are attached to four arms, and the rotational speed of each motor can be set independently, however, only cases with the same rotational speed for all motors are reported in this paper.

The aims of each model can be summarized as follows ;

- Box0012 and Box0012_flap: The box wing evaluated in our previous wind tunnel experiments [4] used NACA0012 airfoil set parallel to the propeller axis. Therefore, similar Box0012 set as the standard box wing configuration.
- Box2421 and Box2421_flap: The airfoil is set 20 degrees downward to the propeller axis reflecting the previous flight test. Since the experimental results of the flight model shown in Figure 2 indicated that transition flights could be more easily performed by tilting the wing about 20 degrees downward to the propeller axis. It is thought that this was because the angle change from the hovering state to the horizontal flight state is smaller and that the drag near hovering condition was smaller. In addition, for higher stiffness and strength with a thicker airfoil section and a higher coefficient of maximum lift, a NACA2421 airfoil is used as improved configurations.
- Wing2421: The same airfoil section as Box2421 was used to see the difference between a box wing and a cantilever wing. The propeller axis and the wing have to be parallel because the propeller and wings are very closely located.

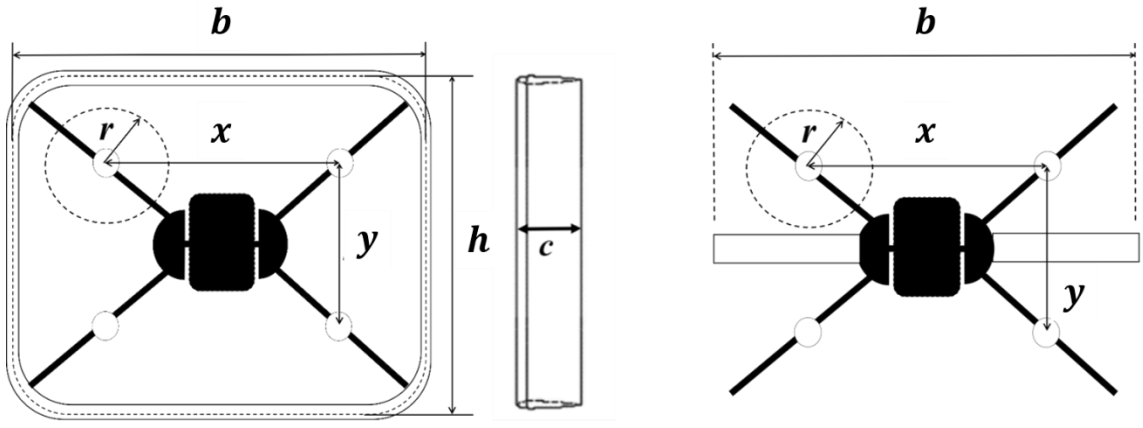

Figure 4 – Frontal Views of wind tunnel models. (Left: Box wing and Right: Cantilever wing)

Table 1 – Dimension and type of the models

Configuration	Box0012	Box2421	Wing2421	NoWing
$Wing\ Type$	Box Wing	Box Wing	Cantilever	—
$Wing\ Span;\ b$[m]	0.700	0.700	0.700	—
$Height;\ h$[m]	0.570	0.570	—	—
$Chord;\ c$[m]	0.1016	0.1016	0.2032	—
$Horizontal\ Propeller\ Distance;\ x$[m]	0.382	0.382	0.382	0.382
$Vertical\ Propeller\ Distance;\ y$[m]	0.254	0.254	0.254	0.254
$Propeller\ radius;\ r$[m]	0.1016	0.1016	0.1016	0.1016
$Reference\ Wing\ Area;\ S$[m^2]	0.14	0.14	0.14	—
$Sectional\ Airfoil\ Type$	NACA0012	NACA2421	NACA2421	—

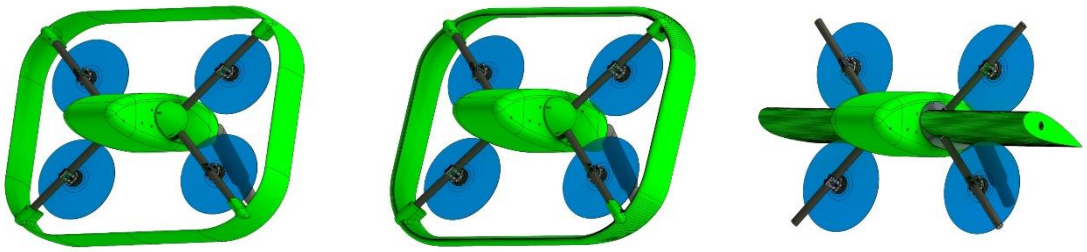

Box0012 Box2421 Wing2421

Figure 5 – Figures of the wind tunnel test models. Blue disks indicate propellers.

2.3 Wind Tunnel Test Results on the Forces and the Moment

Cases with wind speeds of 0 m/s, 10 m/s, and 20 m/s, and propeller rotation speeds of 0 RPM, 5657 RPM, and 8000 RPM were measured for each configuration. The angle of attack varied from 0 to 90 degrees, with the propeller axis parallel to the wind tunnel axis at 0 degrees and perpendicular to the wind tunnel axis at 90 degrees.

The lift, drag, and pitching moment coefficients to the angle of attack characteristics of each configuration for the wind speed of 20 m/s are shown in Figures 6-8.

Each value is obtained by subtracting the value of NoWing from that of the winged configurations. Therefore, these values represent only the aerodynamic force of the wing after subtracting the propeller thrust. In the experiment, however, the propeller thrust should have been affected by the wing, but that effect is ignored here. The changes of propeller thrust are included in the changes of force acting to the wings.

The propeller rotational speeds are shown in the non-dimensional value defined by the following,

$$k = \left(\frac{R\omega}{V} \right)^2 \tag{1}$$

where R, ω and V denote the propeller radius, the angular velocity and the wind speed, respectively.

The corresponding figures for the cases of wind speed of 10 m/s are shown in Appendix A. In each of the 10 m/s wind speed cases, the effect of the propeller is larger due to the larger non-dimensional parameter k, which is qualitatively consistent with the 20 m/s case.

Characteristics that can be read from these results are described below.

- As clearly shown in the difference between (b) and (c-f) in Figure 6, the effect of propeller slipstream is more significant for the Wing2421 than for the Box wings; the trends in drag in Figure 7 and in the moment in Figure 8 are also similar.
- The effects of propeller slipstream are more apparent at high angles of attack of 30 degrees or more. Especially for the Wing2421, the steep changes in lift and moment due to stall disappear in the highest *k(=17.5)* case.
- As shown in (a) and (b) of Figures 6, 7 and 8, the effect of the propeller slipstream on the aerodynamic forces in the lift, drag and moment of Wing 2421 are as large as the size of the propeller thrust itself.

- The effect of propeller slipstream is generally proportional to the parameter *k* for Wing2421. On the other hand, the effects of that on the box wings are smaller, and the proportionality to *k* is not clear.
- As shown in Figure 8, the moment variation of the Box wing is smaller than that of the Wing2421.
- As shown in the comparison between (c) and (d), (e) and (f) in Figure 6, the maximum lift coefficient increases by about 0.3, or about 30%, with the Gurney flap attached.

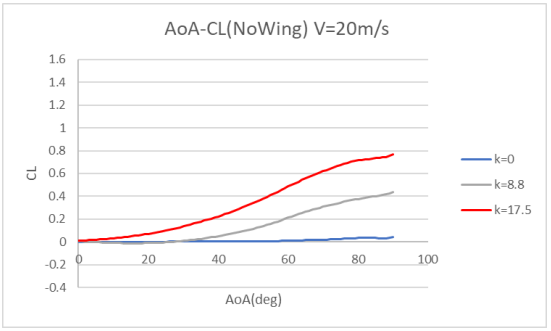

(a) NoWing

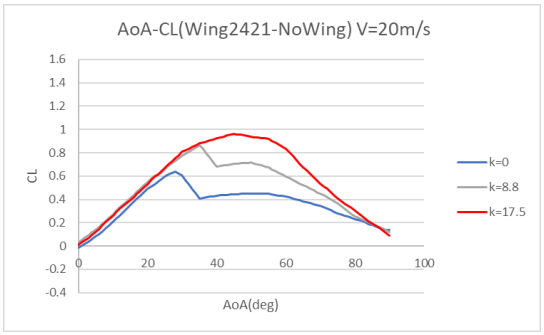

(b) Wing2421

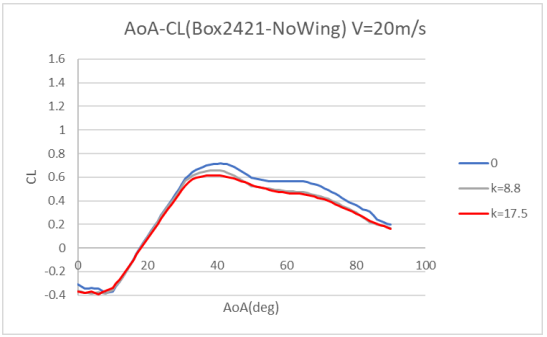

(c) Box2421

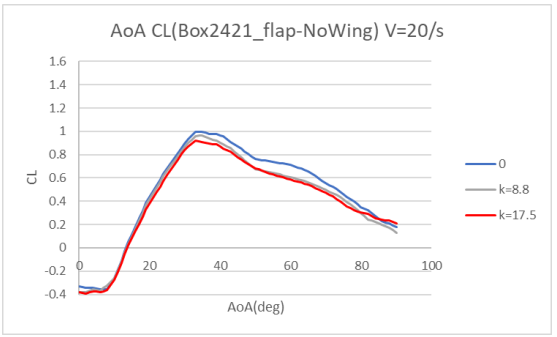

(d) Box2421_flap

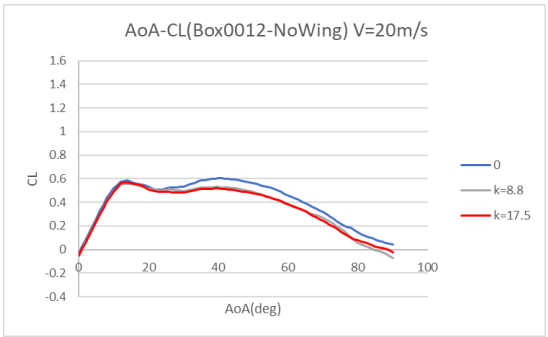

(e) Box0012

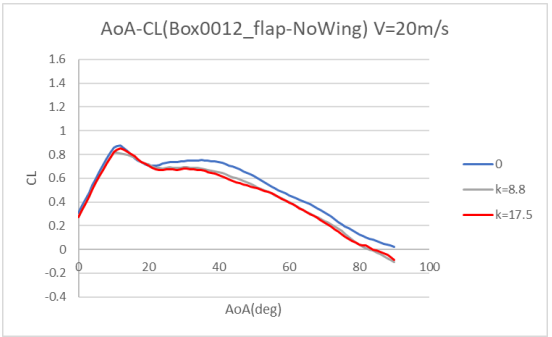

(f) Box0012_flap

Figure 6 – The angle of attack (AoA) to the lift coefficient (CL) characteristics of each configuration at wind speed is 20 m/s. Note that the results are differences from NoWing except for the NoWing results.

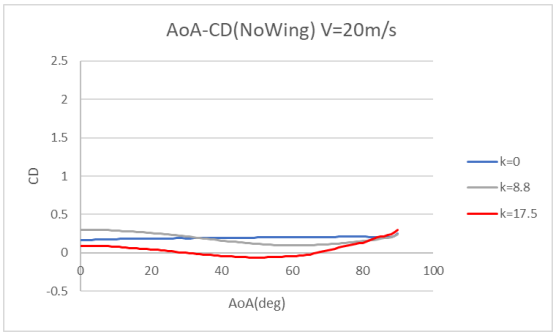

(a) NoWing

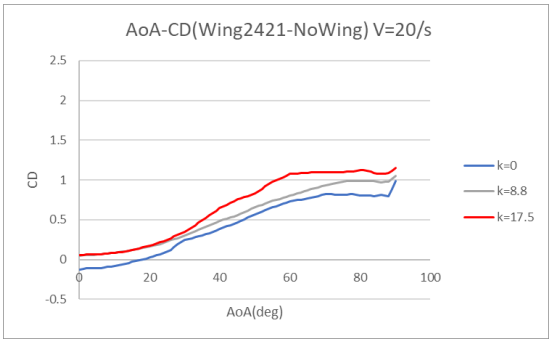

(b) Wing2421

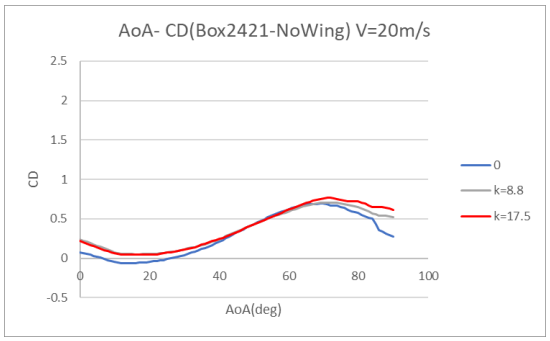

(c) Box2421

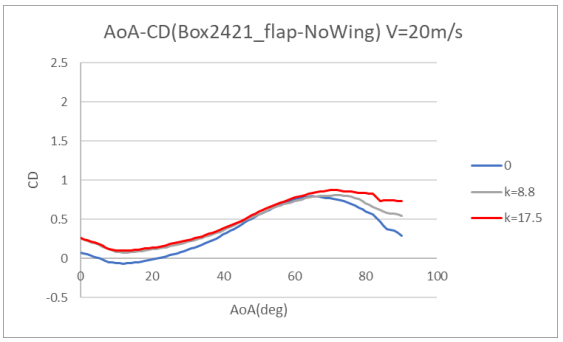

(d) Box2421_flap

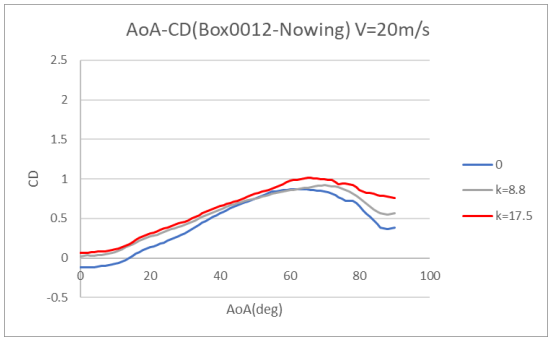

(e) Box0012

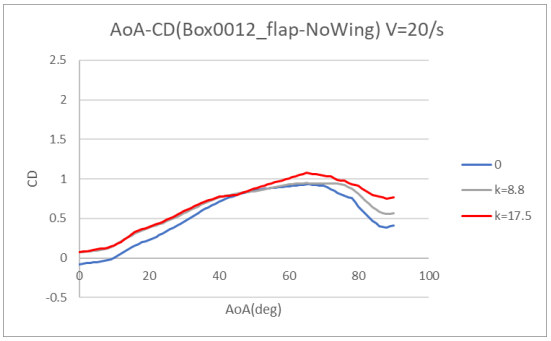

(f) Box0012_flap

Figure 7 – The angle of attack (AoA) to the drag coefficient (CD) characteristics of each configuration at wind speed is 20 m/s. Note that the results are differences from NoWing except for the NoWing results.

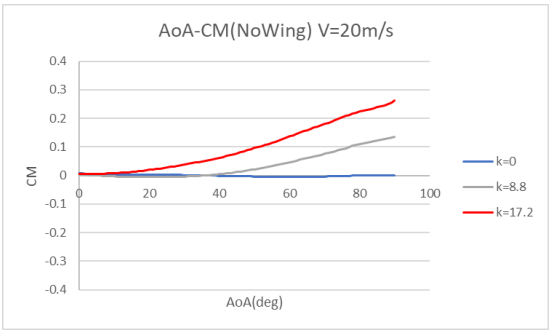

(a) NoWing

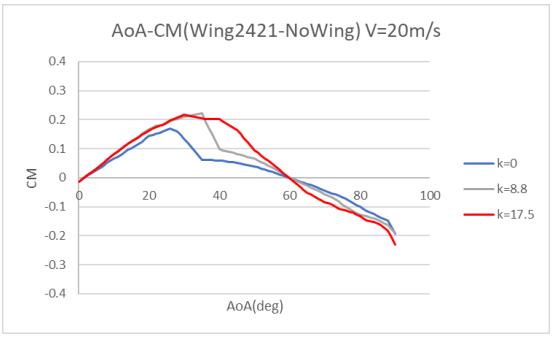

(b) Wing2421

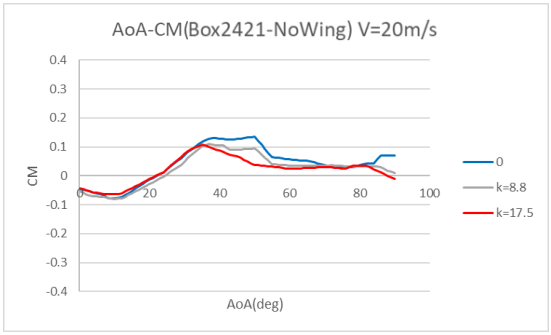

(c) Box2421

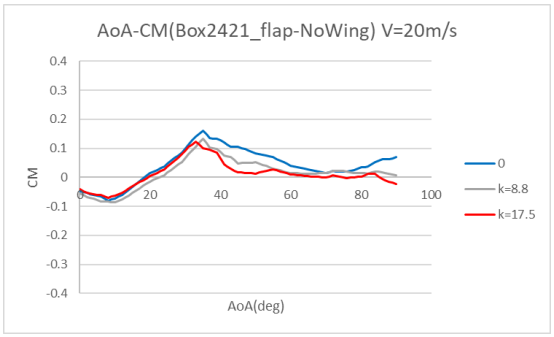

(d) Box2421_flap

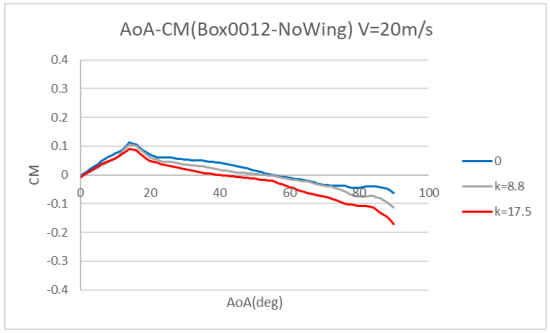

(e) Box0012

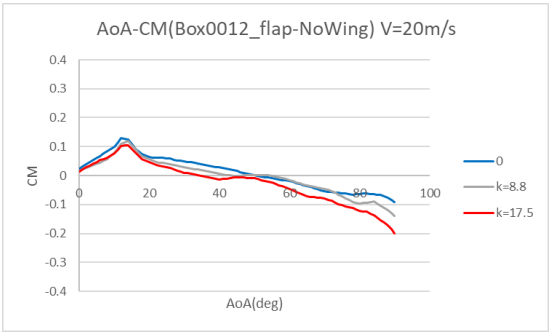

(f) Box0012_flap

Figure 8 – The angle of attack (AoA) to the pitching moment coefficient (C_M) characteristics of each configuration at wind speed is 20 m/s. Note that the results are differences from NoWing except for the NoWing results.

2.4 The Thrust Coefficients and Figures of Merit at Hovering Conditions

The thrust coefficients (C_T) of each configuration under hovering conditions and the figure of merit (FoM), which is the efficiency at hovering conditions, are shown in Figure 9 for the cases of 5700RPM and 8000RPM. C_T and FoM for the aircraft are defined by;

$$C_T = \frac{\sum_{i=1}^{4} T_i}{\sum_{i=1}^{4} \rho \pi R^4 \omega^2} \tag{2}$$

$$FoM = \frac{\left(\sum_{i=1}^{4} T_i\right)^{\frac{3}{2}}}{\sqrt{\sum_{i=1}^{4} 2\rho\pi R^2}} \frac{1}{\sum_{i=1}^{4} W_i} \tag{3}$$

where ρ , T, R , W and ω denote the air density, thrust, radious, power consumption and anguler velocity of each proppeler respectively and subscript “i” denotes index of each propeller. FoM should be unity for the ideal actuator disk and the ideal motor that never exist in reallity.

The energy consumption was calculated from the voltage and current of the motors and that includes heat loss at motors and amps.

For each configuration, higher C_T and FoM are observed in higher RPM cases, so the right endpoints of the line segments correspond to the higher RPM cases. It is thought that it is due to lower friction drag of higher Reynolds number in higher RPM cases.

The box wing can be regarded as an integrated duct, and it is known that both C_T and FoM can be improved by using a properly designed duct. However, for the box wings used in this study, both values are inferior to those for the cantilever wing and the wingless configuration. This may be due to the fact that the appropriate airfoil shape for a wing is not the appropriate cross-section for a duct.

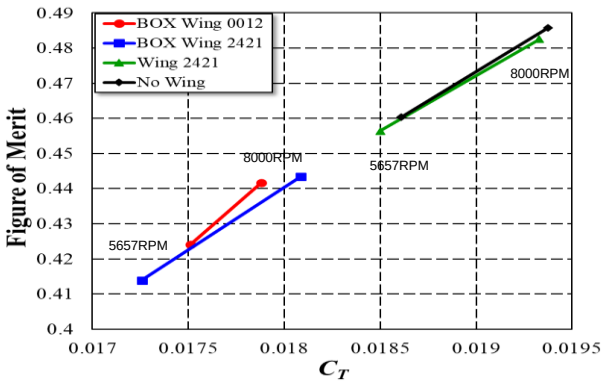

Figure 9 - C_T and FoM of each configuration at hovering condition. 5700RPM case and 8000RPM case for each configuration are shown in the figure.

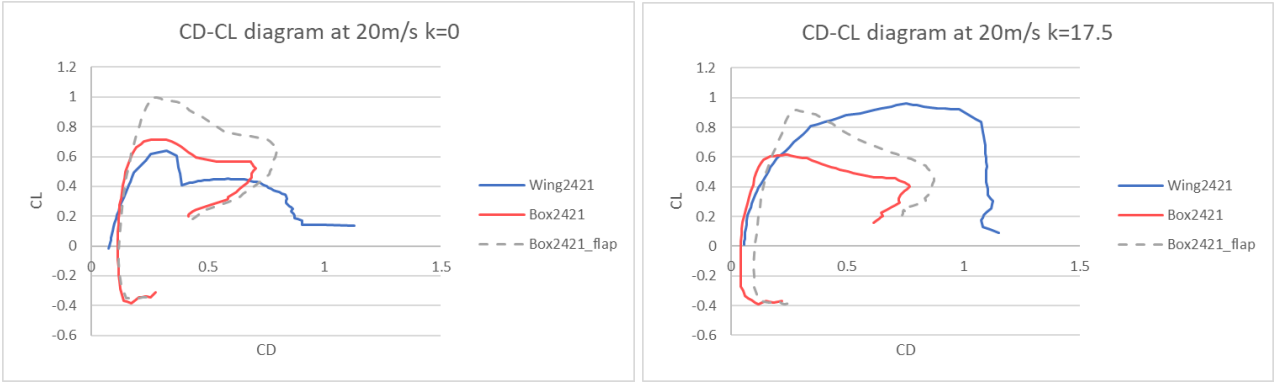

Figure 10 - C_D-C_L diagrams of Wing2421, Box2421 and Box2421_flap for k=0 (left) and k=17.5, i.e., 8000RPM (right).

2.5 Discussion on Aerodynamic Performance

As a representative example of the wind tunnel test results, the C_D-C_L diagrams of Box2421, Box2421_flap, and Wing2421 at wind speed of 20 m/s are shown in Figure 10. It can be concluded that;

- The reference wing area is same for all wings, however, the box wings have larger wetted area due to side wing. Therefore, the minimum drag of Wing2421 is smaller than that of others for no slipstream cases.
- It is known that the aerodynamic drag can be divided into the minimum drag and the induced drag and the induced drag coefficient is proportional to the square of the lift coefficient. The drag of the box wings increases more slowly than that of Wing2421 with the increase of lift. This is due to the improvement of the wing efficiency by the box wing effect. The drag of box wings are less than that of Wing2421 in the range of C_L>0.3 despite the more minimum drag for no slipstream cases.
- The angle of attack increases, and a stall occurs near the C_L of 0.6 to 0.8. The lift of the box wing decreases more gently, indicating that it has a gentle stall characteristic in no propeller slipstream cases. On the other hand, the stall characteristic of Wing2421 becomes very gentle with the propeller slipstream.
- For all forces and moments, the effect of propeller slipstream on Wing2421 is more significant. This is due to the propeller being closer to the wing and the propeller covering most of the surfaces of the wing.
- At the high angle of attack, i.e., from the center to the right side of the figures, the drags of the box wings are about half of that of the Wing2421. This reflects the fact that the frontal projected area at around 90 degrees is about half that of the Wing2421 due to the division of the wing into upper and lower parts. This also means that there is less drag during the transition from hovering to transition flight.

3. Transition Flight from Hovering to Cruising

3.1 Aerodynamic Database

Aerodynamic data obtained in wind tunnel tests are at only limited wind tunnel speed, propeller speed, and angle of attack, so interpolation is necessary to determine characteristics over the entire flight envelope.

Linear interpolation is used for the angle of attack, for which there are relatively many measurement points. For the speed and propeller speed, bi-linear interpolation in the space of ρV^2 and $\rho\omega^2$, where ρ denotes the air density, was used to obtain the forces and moments under each condition.

The experiment was conducted up to a wind speed of 20m and a propeller speed of 8000 RPM, so the results are interpolated within that range, but beyond that, the results are extrapolated, and the accuracy will be reduced.

3.2 Conditions of Steady Horizontal Flight

Using the aerodynamic database, we obtain the conditions for horizontal steady flight by finding a pair of angles of attack, speed, and propeller speed at which the horizontal force is zero and the vertical force is equal to the aircraft weight at each angle of attack.

The wind speed of 20 m/s or less and the rotation speed of 8000 RPM or less are a reliable range for the database, therefore we consider horizontal steady-state flight conditions within this range.

Calculations were made for 1.5 kg and 2.0 kg as the aircraft's weight. 8000 RPM produces about enough thrust to hover for 2 kg aircraft for Box wings.

The relations in horizontal velocity, angle of attack, and RPM are shown in Figures 11-14. The cases for 1.5 kg are shown in the left column, and the cases for 2.0 kg are shown in the right column. The trend is similar in both aircraft weights except for the higher RPM needed for heavier aircraft.

It is shown that only Box0012 and Box0012_flap cannot fly at lower RPM than the hovering condition in Figures 11 and 13. As a result, 2.0 kg aircraft with these wings cannot fly under 8000RPM. There

is a flyable range for other configurations under 8000 RPM. Wing2421 shows a significant decrease of required RPM near hovering conditions.

Box2421 configuration shows the fastest cruise speed in both cases. It indicates that this configuration has the lowest drag in cruise conditions. It is a natural consequence estimated from the lift and drag relation shown in Figure 10.

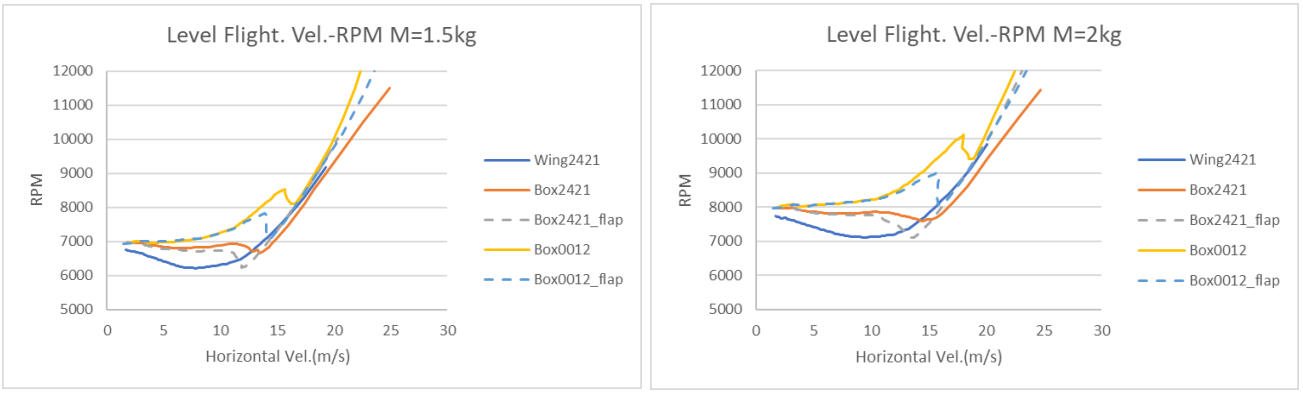

Figure 11 - Diagram of horizontal velocity and RPM in the steady horizontal flight of each configuration with 1.5 kg aircraft(left) and 2.0 kg aircraft(right).

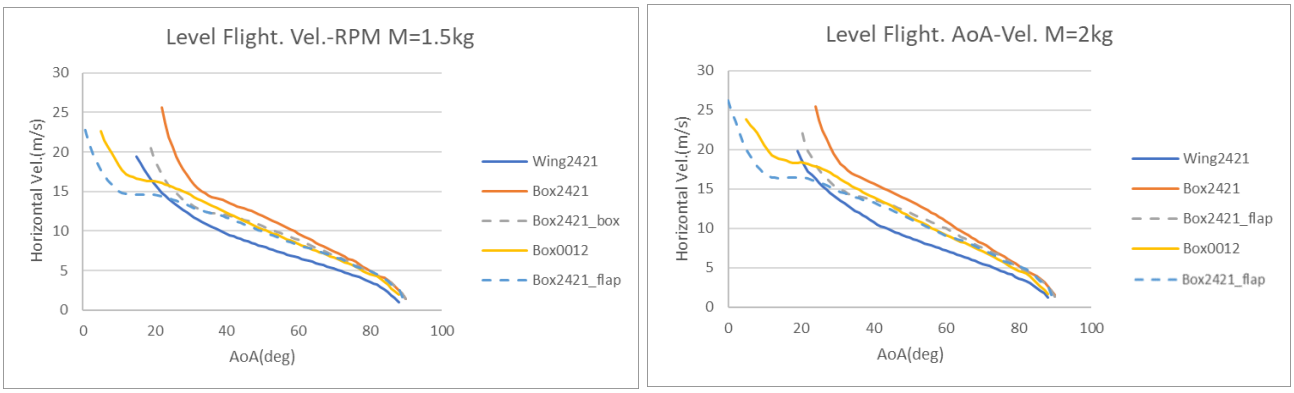

Figure 12 - Diagram of angle of attack and horizontal velocity in the steady horizontal flight of each configuration with 1.5 kg aircraft(left) and 2.0 kg aircraft(right).

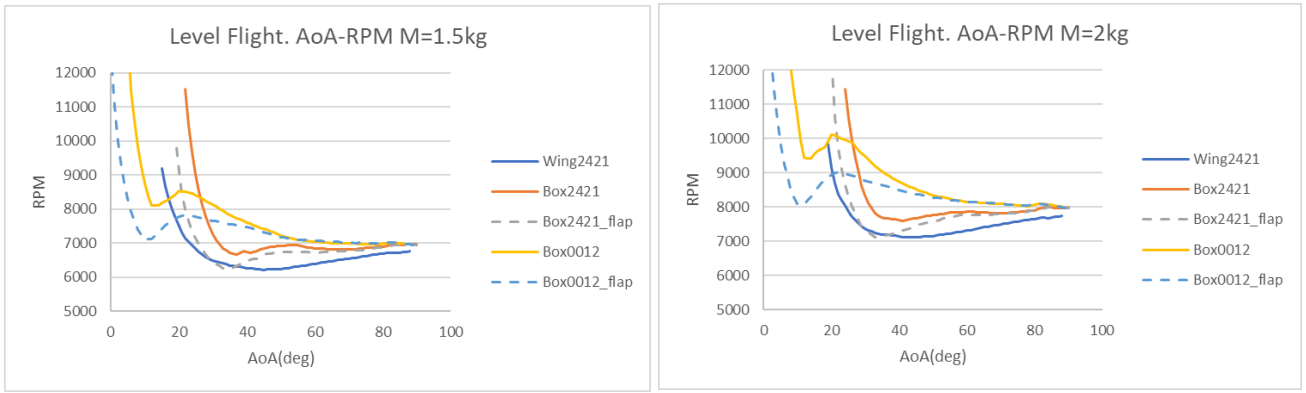

Figure 13 - Diagram of angle of attack and RPM in the steady horizontal flight of each configuration with1.5 kg aircraft(left) and 2.0 kg aircraft(right).

3.3 Simulations of Hover to Cruise Transition Keeping Same Altitude

Using an aerodynamic database, the horizontal force and propeller speed were obtained by specifying velocity, angle of attack, and vertical forces consistent with weight. The equation of motion in the horizontal direction was solved to simulate transition flight from hovering while maintaining horizontal flight.

The relationship between horizontal speed and RPM shown in Figure 14 is quite similar to that for steady horizontal flight shown in Figure11. This fact suggests that the characteristic of slow transition flight can be estimated from those of steady horizontal flight. Box2421 shows the fastest speed and acceleration again in Figure 15 reflecting the lowest drag.

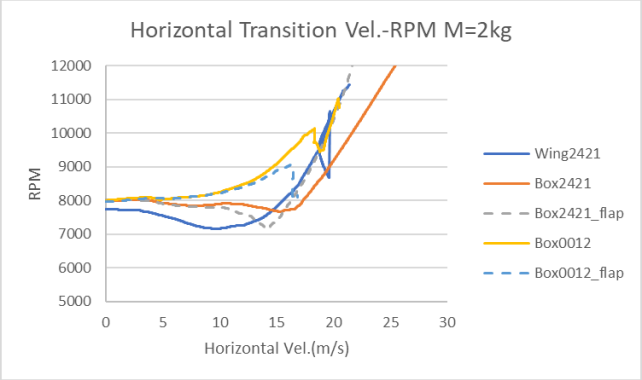

Figure 14 - Relationship between horizontal velocity and RPM in horizontal transitional flight of each configuration with 2.0 kg aircraft.

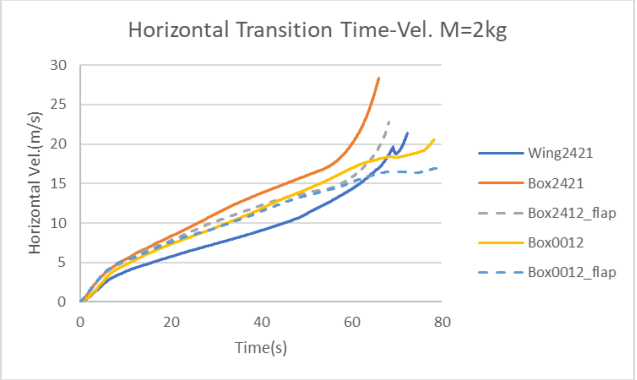

Figure 15 – History of horizontal velocity in horizontal transitional flight of each configuration with 2.0 kg aircraft.

Table 2 – Angle of attack in degree at steady horizontal flight condition at 8000 RPM.

	Wing2421	Box2421	Box2421_flap	Box0012	Box0012_flap
Weight=1.5kg	18.0	27.4	22.0	32.0	5.8
Weight=2.0kg	31.7	26.1	24.1	10.0	12.0

Figure 16 - Transitional flight path maintained at 8000RPM of each configuration with 1.5 kg aircraft(left) and 2.0 kg aircraft(right).

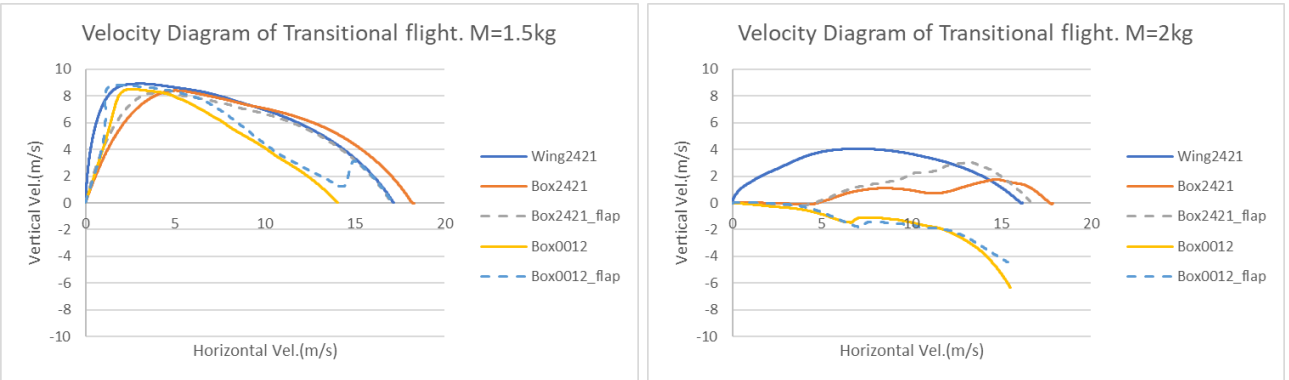

Figure 17 - Diagram of horizontal and vertical velocity in transitional flight maintained at 8000RPM of each configuration with 1.5 kg aircraft(left) and 2.0 kg aircraft(right).

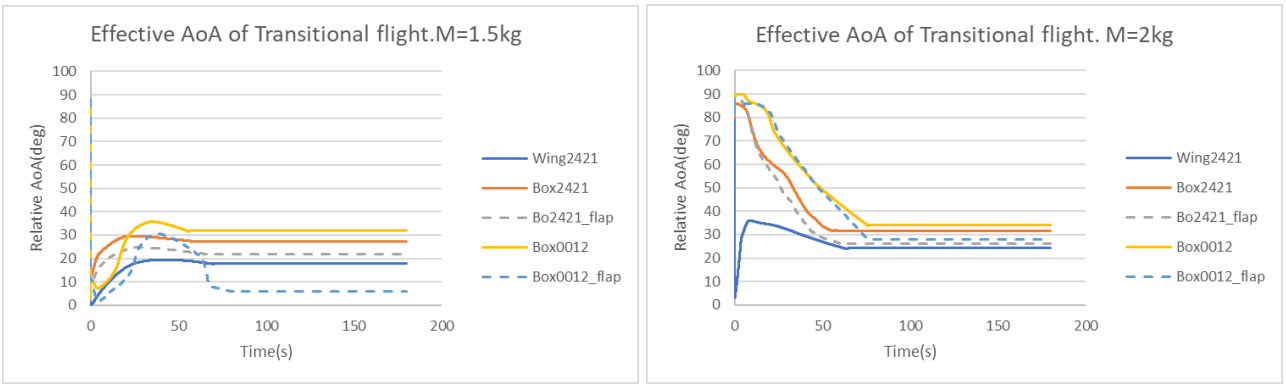

Figure 18 – History of the relative angle of attack to the temporal flow direction in transitional flight maintained at 8000RPM of each configuration with 1.5 kg aircraft(left) and 2.0 kg aircraft(right).

3.4 Transitional Flight Keeping Propellers Rotation at 8000 RPM

Transitional flight from hovering to horizontal steady flight was simulated with the propeller speed fixed at 8000 RPM and the aircraft weight assumed to be 1.5 kg and 2.0 kg. The attitude angle was varied by 1.0 deg/s, up to the angle of attack that allows horizontal cruising at 8,000 RPM determined in the previous section shown in Figure 13. The final angles of attack are shown in Table 2. As there are no steady horizontal flight conditions at 8000 RPM and 2.0 kg for Box0012norr Box0012_flap, angles of attack give local minimum RPMs are chosen, those indicates by the * mark in the table. Note that the effective angle of attack of Box2421 and Box2421_flap is 20 degrees less because their wings face 20 degrees downward.

The maximum altitude gain of 500 m during the transition flight, as shown in the flight path in Figure 16, is not practical for small drone operations. Although an angular change of 1.0 deg/s was assumed here, a faster angular change should be used.

All of the 1.5 kg aircraft and the 2.0 kg aircraft with Wing2421 climb at a near-vertical angle at the beginning of the transitional flight, while the 2.0 kg aircraft with Box2421 and Box2421_flap accelerates while maintaining a horizontal flight, as shown in Figure 16. As a result, the relative angle of attack is suppressed to a small value for the aircraft that climbs vertically in the initial stages of transition flight, as shown in Figure 18. In contrast, the relative angle of attack is closer to 90 degrees for aircraft that maintain level flight at the initial stage.

3.5 Discussion on Transitional Flight

As mentioned in the previous section, the transition was possible in all configurations if the aircraft weight was 1.5 kg. 2.0 kg of aircraft weight is roughly balanced with hovering thrust, so the ratio of hovering thrust to weight for a 1.5 kg aircraft is more than 1.3, indicating that transition flight is possible with a thrust-to-weight ratio of this magnitude.

Wing2421, Box2421, and Box2421_flap can perform transition flight while maintaining horizontal flight, making them suitable for small drone operations, while Box0012 and Box0012_flap have upright wings and high drag near the hovering state, making acceleration from the hovering state difficult. Box2421 and Box2421_flap have a wing angle of 20 degrees, which makes it easier to accelerate with less drag near the hovering state. In addition, Wing2421 has a propeller slipstream effect that suppresses flow separation at high angles of attack, and it has superior propeller propulsion efficiency as shown in 2.4.

Angles of attack for steady horizontal flight for Box2421 and Box2421_flap shown in Table 2 looks quite large, however, it is effectively 2.0 to 7.4 degrees, which is not peculiar, considering that the wing is 20 degrees downward. On the other hand, the net values of 18.0 and 31.7 degrees for Wing2421 are extremely large. As shown in Figure 6(b), this is because the stall is suppressed due to the influence of the propeller slipstream in close proximity. The large effects of propeller slipstream are not seen on the box wings.

The relationship between horizontal speed and RPM in horizontal transition flight shown in Figure 14 is quite similar to that for steady horizontal flight shown in Figure11. This fact suggests that the characteristic of slow transition flight can be estimated from those of steady horizontal flight. Box2421

shows the fastest speed and acceleration in Figure 15 reflecting the lowest drag.

Box2421 configuration shows the fastest cruise speed in both 1.5 kg and 2.0 kg aircraft cases. It indicates that this configuration has the lowest drag in cruise conditions. Box2421 is also the fastest in horizontal acceleration, as shown in Figure 15. These are natural consequences estimated from the lift and drag relation shown in Figure 10.

4. Conclusion and Future Work

The aerodynamic characteristics of a multicopter enclosed by a box wing configuration for application to an innovative Electric Vertical Take-off and Landing (eVTOL) aircraft were investigated using wind tunnel experiments.

Wind tunnel experiments revealed that the box wing has characteristics suitable for convertible VTOL, which cruises using the lift of the wing, compared to a normal cantilever wing of the same wing area and span, such as low drag at cruise, gentle stall characteristics, and ease of transition flight due to low drag in a near hovering attitude.

Comparison through wind tunnel tests also revealed that in the box wing configurations, tilting the wing direction 20 degrees downward from the propeller axis is effective for smooth transition flight. This is expected to facilitate the operation of small drones by enabling transition flight while maintaining horizontal flight.

Although it is known that the high-lift performance of Short Take-off and Landing (STOL) aircraft is enhanced by the proximity propeller slipstream, its effect on the box wings is small. On the other hand, for the cantilevered wing used for comparison, the effect of the propeller slipstream is so large that the change in wing lift is comparable to the propeller thrust.

One drawback of the box wing is its low coefficient of thrust (C_T) and efficiency (FoM) during hovering. The box wing investigated here can be regarded as a kind of duct, and it is known that C_T and FoM can be improved by the use of an appropriate duct, but it is thought that the wing profile designed with an emphasis on cruise performance was not appropriate for the duct cross-section. However, hovering is only a small part of the total flight time of a convertible VTOL, so the effect on the overall performance will be not significant.

This research aimed to apply the results to the Passive Pendulum Body (PPB) configuration (as we named it), which does not have a wing actuation mechanism, in order to realize a lightweight and high-performance convertible VTOL. However, the results of this study can also be applied to the tilt-wing configuration in which the wings are actively actuated.

Future work includes investigating the trim capability, power consumption during horizontal and transitional flight, and moment control capability by the differencing propeller thrusts that is the characteristic of the PPB configuration.

CFD analysis to understand the complex flow field around these aircraft will be another future work. Finally, we show a trial of CFD analysis by the implicit large eddy simulation for a wing similar to Box 0012 without propeller at an angle of attack of 25 degrees.

The spanwise distribution of lift coefficient and drag coefficient obtained by the CFD computation are shown in Figure 19. Significant difference between upper and lower wing and spanwise change of both values are observed.

The flow field is visualized by the second invariant of the velocity gradient tensor (Q value), which well indicates the spatial vortex distribution, in Figure 20. It is shown on the left of Figure 20 that there is no qualitative difference between upper wing and lower one at the center part, but there is a remarkable difference at the corners. We can see the longitudinal vortex structure on the right of Figure 20 which is often found in the separated flow on the delta wing and is known to suppress the flow separation. The formation of this vortical flow is due to a complex combination of flow along the side wing and detached vortexes and could make different behaviors of the upper and the lower wing.

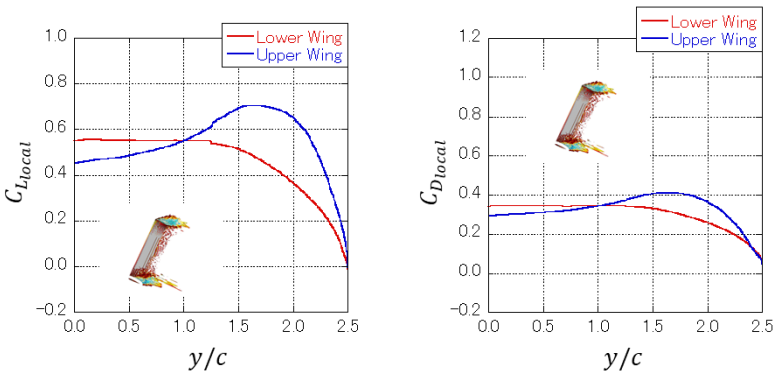

Figure 19 – Spanwise distributions of local lift coefficient (left) and obtained local drag coefficient (right) by CFD.

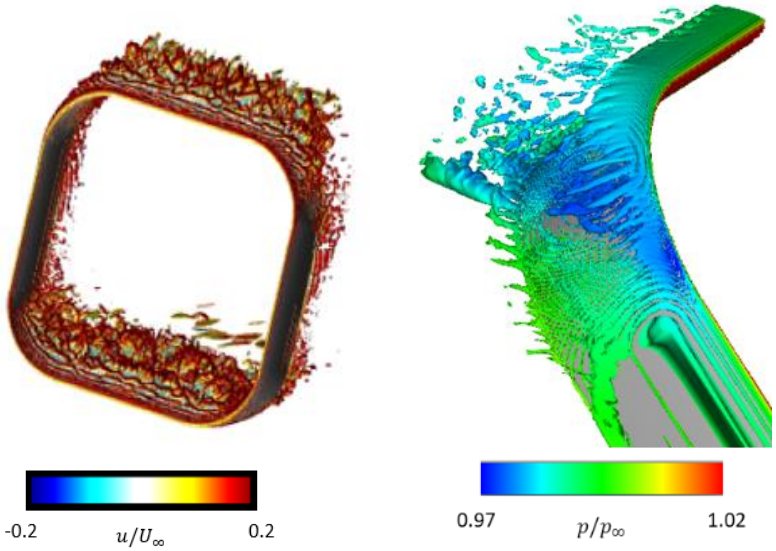

Figure 20 - Spatial distributions of the Q value at 25 degrees. The figure on the left shows the entire wing and contour surface is colored at local velocities. The figure on the right is an enlarged view of the upper corner, in which contour surface is colored with normalized pressure.

5. Contact Author Email Address

mailto: shima.eiji@jaxa.com

6. Copyright Statement

References

[1] Shima E, Tsutsumi S, Fijimoto K and Ito H. Passive Pendulum Body: Proposal of a Novel eVTOL Configuration. *Proceedings of the 51st Fluid Dynamics Conference / the 37th Aerospace Numerical Simulation Symposium*, (July 1-3, 2019. International Conference Center, Waseda University), Shinjuku-ku, Tokyo, Japan, pp.173-181, 2019. (In Japanese)

[2] Shima E, Tsutsumi S, Fijimoto K and Ito H. Passive Pendulum Body: A Novel eVTOL Configuration. *International Powered Lift Conference 2020*, San Jose, California, USA, 2020.

[3] Desami, L, et al. Invariant formulation for the minimum induced drag conditions of nonplanar wing systems. *AIAA journa*l, 2014, 52.10: 2223-2240.

[4] Shima E, Yonezawa K, Nishida R, Sato M, Tsutsumi and Fujimoto K. Wind Tunnel Testing of a Multicopter with Box Wing. Proceedings of Fluid Dynamics Conference / Aerospace Numerical Simulation Symposium 2020 Online, pp.129-136. 2020. (in Japanese)

Appendix A: Wind Tunnel Results for Cases of Wind Speed is 10 m/s

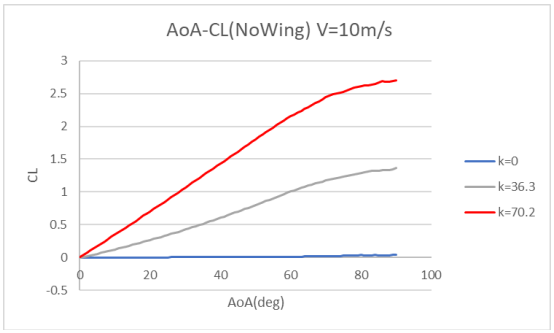

(a) NoWing

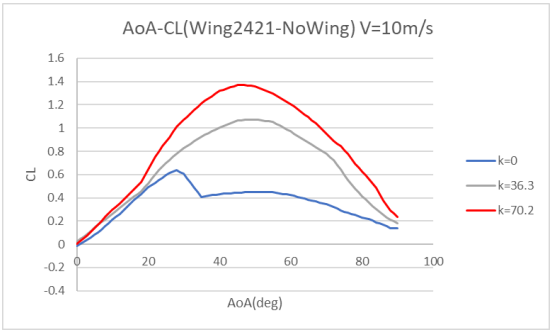

(b) Wing2421

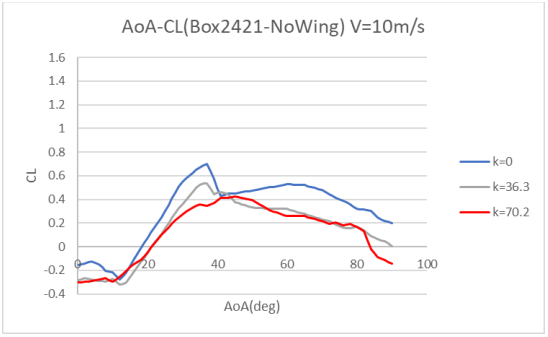

(c) Box2421

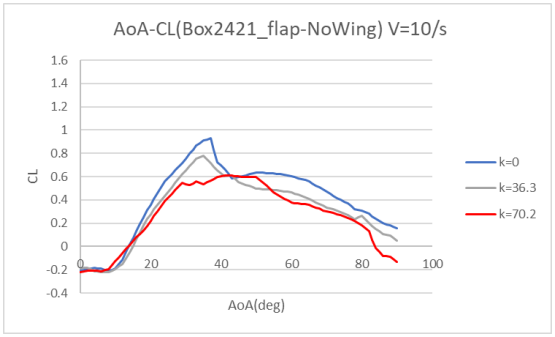

(d) Box2421_flap

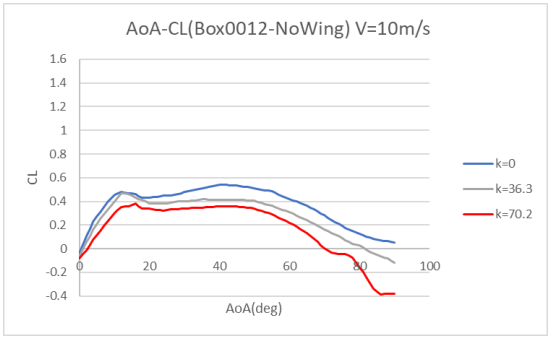

(e) Box0012

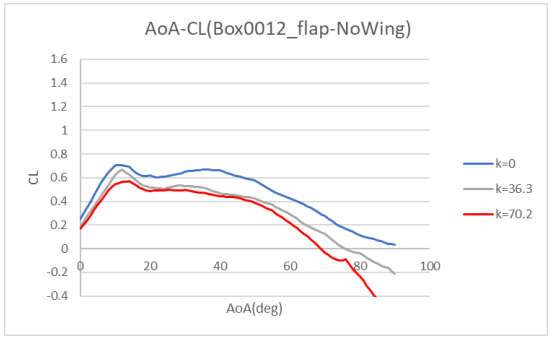

(f) Box0012_flap

Figure A1 – Angle of attack (AoA) to Lift coefficient (C_L) characteristics of each configuration at wind speed is 10 m/s. Note that the results are differences from NoWing except for the NoWing results, and that the scale is different only for the figure (a).

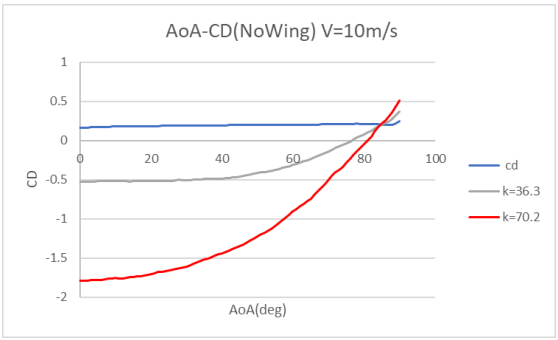

(a) NoWing

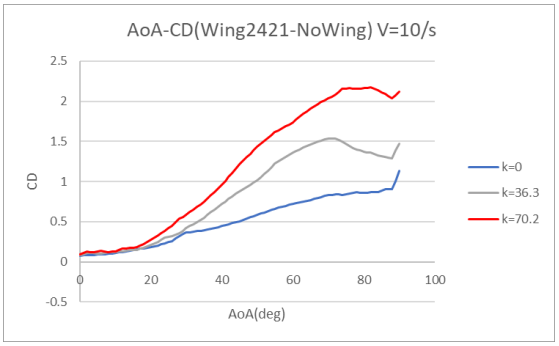

(b) Wing2421

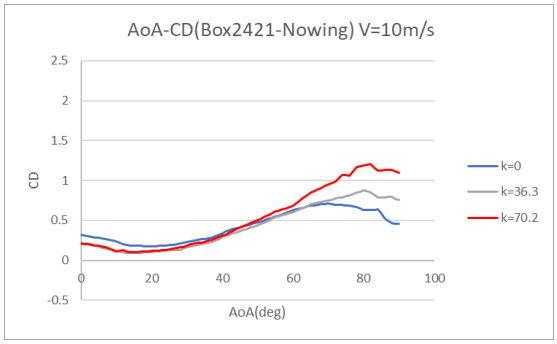

(c) Box2421

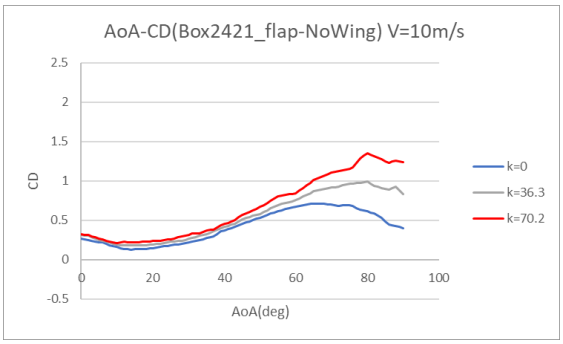

(d) Box2421_flap

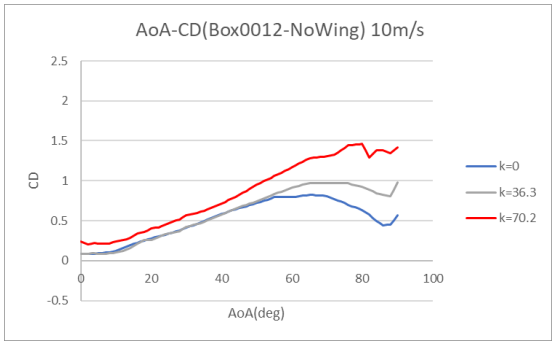

(e) Box0012

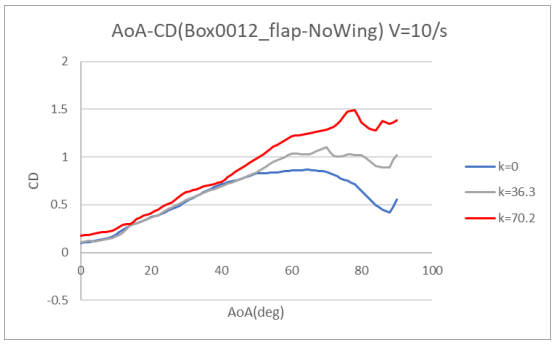

(f) Box0012_flap

Figure A2 – Angle of attack (AoA) to drag coefficient (C_D) characteristics of each configuration at wind speed is 10 m/s. Note that the results are differences from NoWing except for the NoWing results, and that the scale is different only for the figure (a).

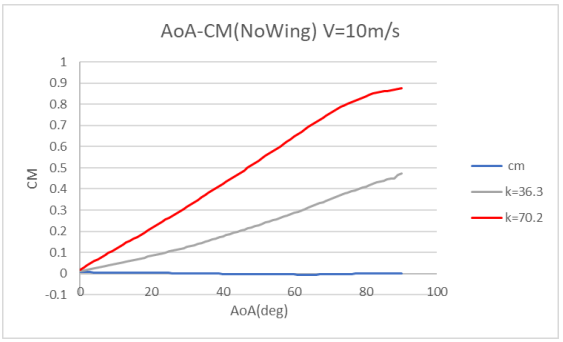

(a) NoWing

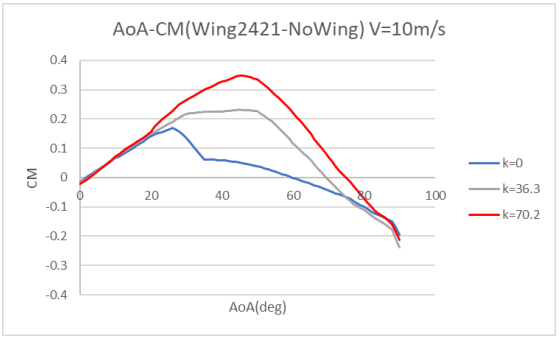

(b) Wing2421

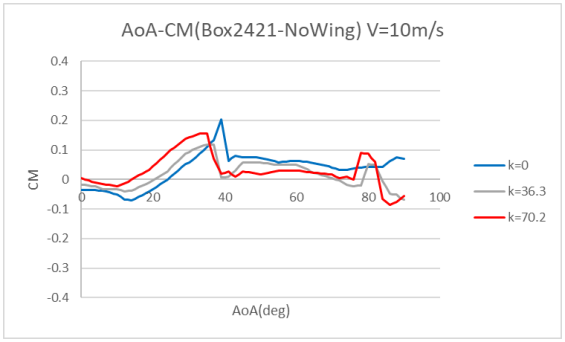

(c) Box2421

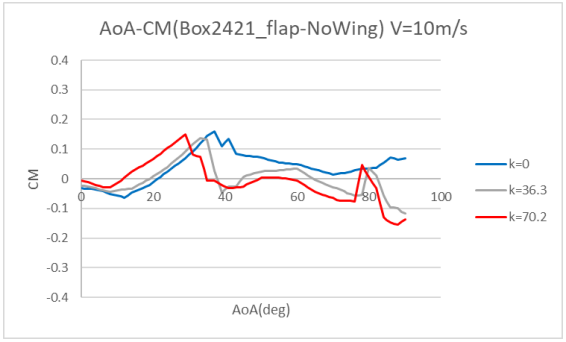

(d) Box2421_flap

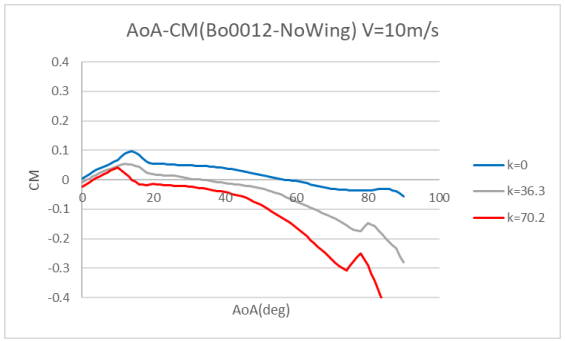

(e) Box0012

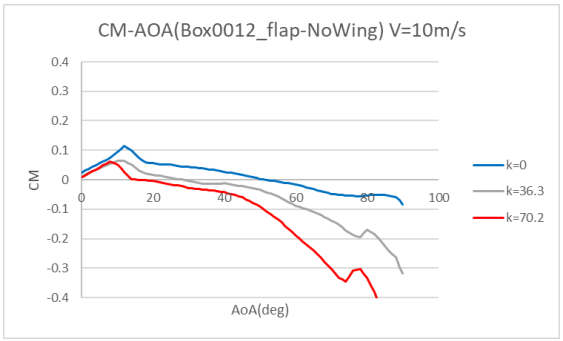

(f) Box0012_flap

Figure A3 – Angle of attack (AoA) to pitching moment coefficient (C_M) characteristics of each configuration at wind speed is 10 m/s. Note that the results are differences from NoWing except for the NoWing results, and that the scale is different only for the figure (a).